Multiqubit subradiant states in N-port waveguide devices: ε-and-μ-near-zero hubs and nonreciprocal circulators

Iñigo Liberal and Nader Engheta

Phys. Rev. A **97**, 022309 — Published 6 February 2018

DOI: 10.1103/PhysRevA.97.022309

Multi-qubit subradiant states in N-port waveguide devices: Epsilon-and-mu-near-zero hubs and nonreciprocal circulators

Iñigo Liberal[1,2] and Nader Engheta[1,*]

[1]Department of Electrical and Systems Engineering, University of Pennsylvania, Philadelphia, Pennsylvania 19104, USA

[2]Department of Electrical and Electronic Engineering, Public University of Navarre, Pamplona, 31006, Spain

*Corresponding author: engheta@ee.upenn.edu

Abstract – Quantum emitters interacting through a waveguide setup has been proposed as a promising platform for basic research on light-matter interactions and quantum information processing. Here, we propose to augment waveguide setups with the use of multiport devices. Specifically, we demonstrate theoretically the possibility of exciting *N*-qubit subradiant, maximally entangled, states with the use of suitably designed *N*-port devices. Our general methodology is then applied based on two different devices: an epsilon-and-mu-near-zero (EMNZ) waveguide hub and a nonreciprocal circulator. A sensitivity analysis is carried out in order to assess the robustness of the system against a number of nonidealities. These findings link and merge the designs of devices for quantum state engineering with classical communication network methodologies.

I. Introduction – The excitation and preparation of multi-qubit entangled states is of fundamental scientific interest as well as the key resource for quantum computing, quantum information processing and quantum metrology [1–6]. Ideally, the ultimate goal is to excite a long-lived state encompassing the entanglement between distant qubits, which requires both long-range interactions and the mitigation of decoherence phenomena [5]. Waveguide setups are particularly well-suited for this purpose [7–13]: On the one hand, long-range interactions are intrinsic to guided modes. On the other hand, the observation of near-unity coupling efficiencies implies that the dissipative coupling with the environment can be canalized into the desired source of interaction. As a matter of fact, although quantum systems inevitably interact with their environment, thus making entanglement inherently fragile [14], dissipative interactions can be designed such that they become the driving force to carry out quantum information processing tasks [15–17]. Indeed, this methodology has been proposed to prepare two-qubit [18–22], mesoscopic [23,24] and macroscopic [25] entangled states, to realize quantum memories [26], quantum repeaters [27] and quantum simulators [28], to perform quantum computation [29] and to generate arbitrary photonic states [30].

Here, we propose augmenting waveguide setups driven by dissipative interactions with the dedicated design of multiport devices. In doing so, we connect the field of quantum state engineering with the communication networking, and subsequently align the fields of reservoir engineering with the design of multiport devices for microwave and optical networks [31]. We expect that this merging of the two concepts will encourage both the adaptation and reutilization of classic multiport devices and the development of innovative devices for quantum state engineering. As a particular example, we demonstrate theoretically the possibility of preparing subradiant multi-qubit states, corresponding to $|W_N\rangle$ states [32], i.e., *N*-qubit maximally entangled states. These subradiant states have also been regarded as a particular class of bound-states in the continuum [33], with applications in lasing, filtering and sensing [33]. We derive a generic procedure for the design of a *N*-port device preparing a *N*-qubit subradiant state, and then we particularize it into two different implementations: a novel epsilon-and-mu-near-zero (EMNZ) two-dimensional (2D) waveguide hub and a conventional nonreciprocal device, a circulator.

Previous studies have investigated the use of multiport devices to engineer quantum interference and generate multiphoton entanglement [34,35]. However, these works are essentially different from our work, where we utilize multiport devices to design dipole-dipole interactions, resulting in the excitation of multi-qubit entangled states.

II. Configuration and generic procedure - A conceptual sketch of the proposed configuration is depicted in Fig. 1: A set of *N* single-mode waveguides are connected via a generic *N*-port device. The response of this device can be described classically by its

scattering matrix $\boldsymbol{S}$, composed by *S*-parameters describing the complex-valued reflection (S_{nn}) and transmission ($S_{nm}, n \neq m$) coefficients at the waveguide ports (see, e.g., Ref. [31]). We assume that there is a quantum emitter (QE), coupled to each of the waveguides at a distance *d* from the multiport device. In the following, the QEs are modeled as identical two-level systems $\{|e_n\rangle, |g_n\rangle\}$ with transition frequency ω_0 and decay rate into the waveguide mode Γ_{wg}.

In a general sense, these distant quantum emitters can be thought to be interacting via photons within a common macroscopic environment, characterized by a given inhomogeneous relative permittivity distribution $\varepsilon(\mathbf{r}, \omega)$, conforming the multiport device and waveguides (see, e.g., Ref. [36–38], Appendix A). Within the Born-Markov approximation, the dynamics of the QE system, characterized by reduced density matrix ρ, is prescribed by the solution of a quantum master equation on its Lindblad form [14,23]: $\partial_t \rho = \sum_{n,m} J_{nm}\left(\sigma_n \rho \sigma_m^\dagger - \rho \sigma_m \sigma_n^\dagger\right) + h.c.$. Here, $\sigma_n = |g_n\rangle\langle e_n|$, and $J_{nm} = -i\frac{\hbar}{\varepsilon_0}\frac{\omega_0^2}{c^2}\mathbf{p}_{\mathrm{n}} \cdot \mathbf{G}(\mathbf{r}_{\mathrm{n}}, \mathbf{r}_{\mathrm{m}}, \omega_0) \cdot \mathbf{p}_{\mathrm{m}}$ are the coupling parameters that describe the environment-mediated interaction between the different QEs (see Appendix A for a derivation of the master equation and coupling parameters). $\mathbf{G}(\mathbf{r}, \mathbf{r}', \omega)$ stands for the classical dyadic Green's function of the macroscopic environment.

Let us assume that we initially excite only one of the QEs such that the initial state of the QE system is given by $|\psi(0)\rangle = \sigma_1^\dagger|0\rangle$. In doing so, we impose that there is a single excitation on the system, and the state of the QE system at any time *t* is restricted to $|\psi(t)\rangle = \sum_{n=1}^{N} c_n(t)\, \sigma_n^\dagger|0\rangle + c_g(t)\ |0\rangle$. In this manner, the number of allowed transitions within the original density matrix is constrained, and the dynamics of the system, described by the aforementioned quantum master equation in Linblad form, are greatly simplified. In particular, we show in Appendix B, that the equation governing the time evolution of the probability amplitudes of the excited states $c_n(t)$ for $n = 1, \ldots, N$, can be simply written in matrix form: $\partial_t \boldsymbol{c}(t) = \boldsymbol{K} \cdot \boldsymbol{c}(t)$, where $\boldsymbol{c} = [c_1(t), \ldots, c_N(t)]^T$ is a vector gathering all probability amplitudes, and $\boldsymbol{K}$ is a square $N \times N$ matrix, whose elements are simply described by the classical Green's function of the macroscopic environment: $K_{nm} = -J_{nm}^*$. For the single mode waveguide system depicted in Fig. 1, we can simply write $K_{nm} = -\frac{\Gamma_{\mathrm{wg}}}{2} S_{nm}\, e^{i2k_{\mathrm{wg}}d}$, for $n \neq m$, and $K_{nn} = -\frac{\Gamma_{\mathrm{wg}}}{2}\left(1 + S_{nn}e^{i2k_{\mathrm{wg}}d}\right)$, where k_{wg} is the propagation constant of the waveguide at the transition frequency ω_0. Less ideal coupling parameters, including, e.g., emission into free-space are considered later.

Formulating the coupling parameters, which describe the QE-interactions mediated through the environment, in terms of classical *S*-parameters enables both the adoption of classic multiport devices (e.g., a circulator) and the dedicated design of new devices (e.g., an EMNZ waveguide hub) for the purposes of reservoir and quantum state engineering. As anticipated, let us illustrate this point with the generation of multi-qubit subradiant states.

For example, let $\{\boldsymbol{g}_p\}$ and $\{\gamma_p = \alpha_p + i\beta_p\}$ be the eigenvectors and associated complex eigenvalues of $\boldsymbol{K}$, respectively. Consequently, we can write $\boldsymbol{c}(t) = \sum_p a_p(t)\boldsymbol{g}_p = \sum_p a_p(0)e^{\gamma_p t}\boldsymbol{g}_p$. It is thus clear that long-term ($t \to \infty$) asymptotic state of the system is defined by the Kernel of $\boldsymbol{K}$, i.e., $\boldsymbol{c}(\infty) = \sum_p a_p(0)\boldsymbol{g}_{0p}$ for $\boldsymbol{g}_{0p} = \boldsymbol{g}_p \in \ker(\boldsymbol{K})$. In other words, the system decays into its initial projection in the decoherence-free subspace (DFS), i.e., a combination of the subradiant or dark states of the system, determined by the initial condition on the QE system $\boldsymbol{c}(0)$. In this manner, and since, $\boldsymbol{K}$ is described by the *N*-port device scattering matrix, one directly recasts the quantum state engineering problem to the design of a conventional waveguide device.

For instance, if the multiport device is designed such that $\ker(\boldsymbol{K})$ is spanned by the state $|W_N\rangle = \frac{1}{\sqrt{N}}\sum_{n=1}^{N} \sigma_n^{\dagger}|0\rangle$ (i.e., $c_1 = c_2 = \cdots c_N = 1/\sqrt{N}$), then the system will eventually decay into $|\psi(\infty)\rangle = \sqrt{P_W}\,|W_N\rangle + \sqrt{1-P_W}\,|0\rangle$. That is to say, the desired state is generated with probability $P_W = |a_W(0)|^2 = N^{-1}$. Interestingly, this probability is independent of the *N*-port device, since it is prescribed by the projection of the initial state into the target state. On the contrary, additional aspects of the process such as the transient time required to reach this state and/or the robustness of the system against nonidealities do depend on the design of the *N*-port device.

Here, it is important to remark that the failure in generating the desired state is heralded by the measurement of a photon at the exit of the waveguides. In other words, measuring a photon during the transient process projects the state of the system $|\psi\rangle = \sqrt{P_W}\,|W_N\rangle + \sqrt{1-P_W}\,|0\rangle$ into $|\psi\rangle = |0\rangle$, while not measuring it projects the state of the system into $|\psi\rangle = |W_N\rangle$. Therefore, the fidelity in preparing the $|W_N\rangle$ can in theory approach one. Naturally, and as it is investigated later, any practical realization will present a number of nonidealities. As a result, the subradiant state will always have a finite lifetime, and the fidelity in generating the state is always in practice smaller than one.

Admittedly, more sophisticated protocols exhibiting higher performance/fidelity could be developed by using more complex (e.g., multi-level) emitters, or excitation configurations (e.g., individually addressing the emitters with a dedicated laser) [39]. Here, we have opted for a simple configuration based on two-level systems in order to further re-emphasize the main conclusion behind this work: part of the complexity behind quantum state engineering processes can be relaxed and transferred to the design of classical waveguide devices. In the next sections we examine two specific *N*-port devices that can be utilized in the generation of these states:

III. Epsilon-and-mu-near-zero (EMNZ) two-dimensional (2D) hubs - Continuous media and artificially engineered structures with near-zero parameters (e.g., EMNZ media, a

medium with near-zero relative permittivity $\varepsilon \approx 0$ and permeability $\mu \approx 0$ [40–42]), exhibit a number of salient features, such as the decoupling of spatial and temporal field variations [42,43], leading to exotic wave dynamics [44]. In particular, waveguide sections filled with EMNZ media enable the perfect tunneling of electromagnetic waves (i.e., a transmission coefficient of unity for the two-port EMNZ scenario) independently of certain geometrical deformations of the transmission channel [45–48]. The decay of and interaction between QEs embedded within ENZ waveguides have also attracted the attention of the researchers [21,49–55]. Interestingly, we find that multiport EMNZ waveguide hubs can also be utilized for the preparation of multi-qubit states via the methodology described in the previous section.

In order to illustrate this point, we consider a two-dimensional (2D) system depicted in Fig. 2a, which consists of an arbitrarily shaped *N*-port EMNZ waveguide hub. Next we derive the *S*-parameters of this device that, owing to the special properties of EMNZ structures, exhibit highly symmetric properties. First, we note that since the magnetic field is constant within this 2D device [47], we have: $S_{nm} = (S_{mm} - 1), \forall m, \forall n \neq m$. Next, since $\mu \approx 0$ the circulation of the electric field must be zero according to Faraday's law, and thus we find $1 + \sum_{n=1}^{N} S_{nm} = 0 \; \forall m$. By exploiting these two conditions, we find that the scattering parameters of an EMNZ hub are: $S_{nn} = \frac{(N-2)}{N} \;\; \forall n$ and $S_{nm} = -\frac{2}{N}$, for $n \neq m$. One important characteristic of this 2D device with *N* equal waveguide ports is that if it is excited from one port with a classical time-harmonic wave, the waves exiting the other ports are identical in magnitude and phase, regardless of the locations and orientations of the ports (see Fig. 2).

Next, if we set $k_{\mathrm{wg}} d = \pi$, the coupling parameters reduce to $K_{nn} = -\Gamma_{\mathrm{wg}}(N-1)/N \;\; \forall n$ and $K_{nm} = \Gamma_{\mathrm{wg}}/N \;\;$ for $n \neq m$. In the matrix form, we have:

$$\boldsymbol{K} = -\frac{\Gamma_{\mathrm{wg}}}{N} \begin{bmatrix} N-1 & -1 & \cdots & -1 \\ -1 & N-1 & & \cdots \\ \cdots & & \cdots & -1 \\ -1 & \cdots & -1 & N-1 \end{bmatrix} \tag{1}$$

It can be readily checked by inspecting the pertinent characteristic equations that the kernel of $\boldsymbol{K}$ is spanned by $|W_N\rangle$. Since this effect appears when the QE decay rate is compensated by the cooperative decay rates, a classical analogue effect to this subradiant or dark state is that when the QEs are replaced by time-harmonic classical point dipoles emitting in phase, no power is exiting the system. This effect is illustrated in Figs. 3b and 3c, which depict snapshots of the magnetic field (H_z component) excited by 2D point dipoles emitting in phase located at the entrance of EMNZ waveguide hubs of N = 3 and N = 4 ports, respectively. The field distributions were computed with a full-wave numerical solver [56].

In this manner, our analysis indicates that if one of the QEs is initially excited, the system will then decay into $|W_N\rangle$ after a transitory time. Alternatively, one can explicitly solve $\partial_t \boldsymbol{c}(t) = \boldsymbol{K} \cdot \boldsymbol{c}(t)$ to keep track of the time-evolution of the probability amplitude of excitation of each QE. This exercise leads to (see Appendix C)

$$c_1(t) = \frac{1}{N}\left[1 + (N-1)\,\mathrm{e}^{-\Gamma_{\mathrm{wg}} t}\right] \tag{2}$$

and

$$c_n(t) = \frac{1}{N}\left[1 - \mathrm{e}^{-\Gamma_{\mathrm{wg}} t}\right], \text{ for } n = 2, \ldots, N \tag{3}$$

Figures 3d and 3e depict a comparison of the time evolution of the probability amplitude coefficients, as compared to the numerical solution of quantum master equation by using the Euler method, for implementations with $N = 3$ and $N = 4$ ports, respectively. It is apparent from the figure that indeed the system decays into the desired subradiant, maximally entangled, state. One interesting aspect of the transitory time is that the time-evolution of the probability amplitude of the QEs initially in the ground state are identical, i.e., $c_2(t) = c_3(t) = \ldots = c_N(t)\ \forall t$. This effect is a consequence of the nonlocal properties of the EMNZ hub. Specifically, since the coupling is independent of the position of the waveguides, it is impossible to discern the evolution between the QEs sharing the same initial conditions.

EMNZ tunneling has been experimentally validated at microwave frequencies by using waveguides at cut-off [46,48] and arrays of dielectric particles [57]. The latter approach have also been recently scaled up to optical frequencies and integrated into a chip [58]. Extending these validated two-port devices to multi-port systems is straightforward, and therefore we believe that the practical implementation of our proposed concept should be within reach of current technology.

For instance, for a possible future experimentation one can consider the following preliminary design of an all-dielectric (and therefore low-loss) implementation of a four-port EMNZ hub, suitable for operation at optical frequencies and integration on a chip, depicted in Fig. 3. Following the design of a two-port device presented in Ref. [55], the systems is designed by using two different photonic crystals, both constructed by using circular rods of radius $r_{1,2}$ and relative permittivity $\varepsilon_p = 12.5$, arranged in a rectangular lattice with period $a_{1,2}$. Specifically, the EMNZ region ($a_1 = 0.56\lambda_0, r_1 = 0.2a_1$) is created by following the design in [57], such that the photonic crystal exhibits a Dirac cone at k = 0, which effectively presents an EMNZ behavior [59]. This region is then bounded by a second PC ($a_1 = 0.56\lambda_0, r_1 = 0.2a_1$) exhibiting a complete band-gap at the frequency of operation. This serves to effectively "close" the system, except for four waveguides and input ports constructed by removing rows of the PC.

Then, this 2D structure is excited with out-of-plane electric current lines ($\boldsymbol{J} = \hat{\boldsymbol{z}}\, I$, shown as blue dots in Fig. 4a), which generate the mode preferably excited for dipole emitters with the transition dipole oriented along the $\hat{\boldsymbol{z}}$ direction. It can be readily checked via numerical simulations [56] that this synthetic device does indeed effectively behave as the previously studied homogeneous EMNZ hub. For example, if only one of the sources is activated (see Fig. 4b), the outgoing waves through all the three remaining ports are identical in phase and magnitude. Moreover, if all sources are excited at the same time (see Fig. 4c), the excited fields correspond to a subradiant or dark state, and there are no outgoing waves (nor power) exiting the system. As anticipated, this is the classical counterpart of mapping a $|W_N\rangle$ state into the decoherence-free subspace of the system. This preliminary design suggests that in the future the proposed configuration could be implemented in practice in an all-dielectric platform.

IV. Nonreciprocal hub: Circulator- Our generic procedure could be implemented by using a variety of devices, including classical waveguide devices that have been developed for entirely different applications. For example, circulators are essential components of microwave [60], millimeter wave [61] and optical–fiber networks [62]. As schematically depicted in Fig. 5a, an ideal circulator can be defined as a matched nonreciprocal device that enables one-to-one unidirectional nonreciprocal transmission. Consequently, the only nonzero elements of the scattering matrix are $S_{1N} = 1$ and $S_{n(n-1)} = 1$ for $n > 1$ (see Fig. 5a). Note that in general the scattering parameters of a circulator might incorporate a phase factor (e.g., $S_{1N} = e^{i\varphi_{1N}}$). However, these phase factors can be easily removed by defining the position of the input ports of the circulator at the planes when the phase factors vanish. In this case, and if the separation between the QEs and the input ports is set to $k_{\mathrm{wg}} d = \pi/2$, then the coupling parameters can be written in matrix form as follows

$$\boldsymbol{K} = -\frac{\Gamma_{\mathrm{wg}}}{2}\begin{bmatrix} 1 & 0 & \cdots & 0 & -1 \\ -1 & 1 & 0 & \cdots & 0 \\ 0 & -1 & \cdots & \cdots & \cdots \\ \cdots & \cdots & \cdots & \cdots & 0 \\ 0 & \cdots & 0 & -1 & 1 \end{bmatrix} \tag{4}$$

Again, it can be readily checked that $\ker(\boldsymbol{K})$ is spanned by $|W_N\rangle$. Alternatively, the time-evolution of the probability amplitudes can be found by explicitly solving the master equations, leading to (see Appendix D)

$$c_n(t) = \tfrac{1}{N}\textstyle\sum_{m=0}^{N-1} \exp\left[-\frac{\Gamma_{\mathrm{wg}}}{2}\left(1 - e^{im\frac{2\pi}{N}}\right)t + im\,2\pi\frac{N-n+1}{N}\right] \text{ for } n=1, \ldots, N \tag{5}$$

Figs. 5b and 5d depict a comparison of the time-evolution of the probability amplitudes obtained via numerical solution of the quantum master equation and Eq. (5), for circulators with $N = 3$ and $N = 4$ ports, respectively. As expected, the system again decays into $|W_N\rangle$ with probability N^{-1}. However, the time-evolution of the $c_n(t)$ coefficients is substantially different from those of the EMNZ waveguide hub. In fact, in this case, the probability amplitudes of the initially non-excited emitters are not identical, and the transient time required to generate the entangled state is slightly longer. This difference arises from the restriction to one-to-one interactions within a circulator. This analysis reveals that *N*-port devices could be engineered to optimize the desired transient time required to generate the entangled state. This and other optimization efforts that could be applied to *N*-port devices are beyond the scope of the present work.

This setup could be implemented in a variety of platforms. Indeed, conventional circulators are widely used in communication and sensor networks, and they are commercially available in microwave, millimeter waveguides and optical fibers [63]. Alternative realizations of circulators have also been proposed in photonic crystal [64] and plasmonic [65] platforms. Moreover, recent advances in chiral photonic circuits when combined with nonreciprocal structures (e.g., an atom exhibiting Zeeman sublevels) might point to ideas and scenarios with efficient and on-chip non-reciprocal photonic elements [66–68], including the recent demonstration of a circulator [69]. In addition, an acoustic circulator has been recently experimentally demonstrated [70]. Therefore, the proposed configuration could also be extrapolated to other physical systems.

V. Beyond the ideal case – In previous sections dealing with ideal cases, the initial excitation probabilistically decays into a multi-qubit entangled state, which is a subradiant or dark state mapped into the DFS of the system, and therefore it remains there for an indefinite time. Moreover, since the failure in generating the state is heralded by a photon exiting the system in the waveguides, the fidelity in generating the entangled state theoretically approaches one. Admittedly, any practical realization of the proposed configurations will present a number of nonidealities. As a result, the subradiant state will always exhibit a finite lifetime, and the fidelity in generating the state will always be smaller than unity. Typical nonidealities in the system might include undesired decay processes (e.g., irreversible decay into free-space, dissipation into the environment and/or internal decays within the QEs), imprecision in positioning the emitters, and deviations from the prescribed scattering parameters of the N-port devices, due to deviations from the ideal material parameters and/or fabrication tolerances.

In this section we carry out a sensitivity analysis in order to estimate the robustness of our system against these nonidealities. To this end, we introduce phenomenological coupling parameters for the interaction via a imperfect single-mode waveguide, given by: $K_{nn} =$

$-\frac{\Gamma_{\mathrm{tot}}}{2}\left[(1-\beta)+\beta\left(1+S_{nn}e^{i2k_{\mathrm{wg}}d_n}\right)\right]$ and $K_{nm}=-\beta\frac{\Gamma_{\mathrm{tot}}}{2}S_{nm}e^{i2k_{\mathrm{wg}}(d_n+d_m)}$ for $n\neq m$. Here, β is the usual β-factor [11], which characterizes the efficiency in the coupling of the QE to the desired waveguide mode: $\Gamma_{\mathrm{wg}}=\beta\Gamma_{\mathrm{tot}}$. Note that the distances of each individual emitter to its closer port have been explicitly included to account for errors in positioning them. Deviations from the ideal scattering parameters can be simply taken into account when evaluating them.

In our analysis, we model the QE β-factors as $\beta_n=0.95+0.01\Delta\beta_n$, $n=1,\dots,N$, with $\Delta\beta_n$ following a standard normal distribution. These can be considered realistic values, for example, for QDs inserted in photonic crystal waveguides, where near unity coupling parameters ($\beta=0.9843\pm0.0004$) have been reported [71]. Similarly, inaccuracies in positioning the emitters are modeled as $r_n=\frac{\lambda_{\mathrm{wg}}}{2}(1+0.05\,\Delta r_n)$ with Δr_n following a standard normal distribution. To finalize, we include deviations in the scattering parameters as variations in the magnitude of the transmission coefficients $|S_{nm}|=(0.95+0.01\,\Delta S_{nm})\left|S_{nm}^{i}\right|$, where S_{nm}^{i} is the ideal transmission coefficient, and ΔS_{nm} is again modeled with a standard normal distribution. Physically, this model corresponds to a well-matched device, which however exhibits a certain insertion loss due to dissipation, scattering or mode conversion; which is commonly the case in optical waveguide devices. Without loss of generality, inaccuracies in the phase of the scattering coefficients can be considered included in the positioning of the QEs. We remark that different random distributions are used for the parameters of each of the emitters β-factors, position, and scattering parameters. In this manner, the impact of a lack of symmetry in the coupling between the emitters induced by nonidealities in the systems is taken into account in the sensitivity analysis.

As in previous sections, we compute the dynamics of the system via the quantum master equation, repeat the simulation $M=5\times10^4$ times, and use the data to evaluate the performance of the system. First, we compute the time-evolution of the probability of the initial excitation remaining in the QE system, $P_e(t)=\sum_{n=1}^{N}|c_n(t)|^2$. Fig. 6(a) depicts a comparison between the ideal and nonideal cases, for an EMNZ hub of $N=4$ ports. In the ideal case, the time evolution adjust to the theoretical result: $P_e(t)=\frac{N-1}{N}\,e^{-2\Gamma_{\mathrm{wg}}t}+\frac{1}{N}$, corresponding to a transient decay process with decay rate twice the individual decay into the waveguide, $2\,\Gamma_{\mathrm{wg}}$, and the excitation of a subradiant state with (ideally) infinite lifetime. On the other hand, the values obtained in the sensitivity analysis correspond to the combination of a fast decay during the transitory time, and a slower decay associated with the finite lifetime of the subradiant mode. Specifically, we find that $P_e(t)$ accurately fits to $P_e(t)=\frac{N-1}{N}\,e^{-\Gamma_1 t}+\frac{1}{N}\,e^{-\Gamma_2 t}$, with $\Gamma_1=1.85\,\Gamma_{\mathrm{wg}}$ and $\Gamma_2=0.125\,\Gamma_{\mathrm{wg}}$. We emphasize that the transient decay process is more than one order of magnitude faster than the decay of the

subradiant decay, $\frac{\Gamma_1}{\Gamma_2} = 14.8$, and, therefore, we are optimistic that the multiple decay processes could be observed experimentally, evidencing the excitation of a multi-qubit subradiant state.

Even if the subradiant states can be experimentally observed, one might wonder if they can be generated on demand. In this regard, the presence of multiple decay paths also limits the fidelity with which the subradiant state is prepared. In the ideal case, the system at long times decays into $\lim_{t\to\infty}|\psi(t)\rangle = \left(\sqrt{P_W}\,|W_N\rangle + \sqrt{P_{WG}}\,|0\rangle\right)/\left(\sqrt{P_W + P_{WG}}\right)$. In addition, since in the ideal case the only decay path is the waveguide mode, not measuring a photon at the outputs of the waveguides projects the state of the system into $\lim_{t\to\infty}|\psi(t)\rangle = |W_N\rangle$, which trivially results in a unit fidelity, $\mathcal{F} = |\langle W_N|\psi(t)\rangle|^2 \to 1$. However, in practice, the waveguide mode is not the only decay path, and not measuring a photon projects the system into a superposition of $|W_N\rangle$ and a state in which the photon has irreversibly decayed via a different decay path, necessarily resulting in fidelities smaller than unity in the process of generation of the $|W_N\rangle$ state.

A limitation of our formalism is that, in computing the reduced density matrix for the QE system, the different decay paths cannot be easily resolved. This is first due to the fact that the photonic environment in which the QEs interact is modeled as a common macroscopic bath encompassing all decay paths, and, secondly, because any information on the bath is lost when tracing out the electromagnetic degrees of freedom (see Appendix A).

Despite this fact, a lower bound of the expected fidelity can be estimated under some reasonable assumptions. To this end, an ansatz of the state of the system at time t can be written as follows: $|\psi(t)\rangle = \sum_{n=1}^{N} c_n(t)\sigma_n^\dagger|0\rangle + \sqrt{P_{\mathrm{wg}}(t) + P_{\mathrm{loss}}(t)}\,|0\rangle$, with $P_e(t) + P_{\mathrm{wg}}(t) + P_{\mathrm{loss}}(t) = 1$ at any time t. Here, we have split the probability all QEs being in the ground state to discriminate between P_{wg} (waveguide decay) and P_{loss} (additional decay paths). In this case, not measuring a photon at the output of the waveguides projects the system into $|\psi(t)\rangle = (P_{\mathrm{e}}(t) + P_{\mathrm{loss}}(t))^{-1/2}\left[\sum_{n=1}^{N} c_n(t)\sigma_n^\dagger|0\rangle + \sqrt{P_{\mathrm{loss}}(t)}|0\rangle\right]$. As anticipated, our difficulty in studying the fidelity of the process stems from the lack of knowledge of $P_{\mathrm{loss}}(t)$. However, an upper bound on $P_{\mathrm{loss}}(t)$, and thus a lower bound on the fidelity $\mathcal{F}$, can be obtained by assuming that the probability of decay into the waveguide is larger than that of the ideal configuration, i.e., $P_{\mathrm{wg}}(t) \geq P_{\mathrm{wg}}^i(t) = 1 - P_{\mathrm{e}}^i(t)$. This assumption is particularly conservative after the transient time, since $P_{\mathrm{wg}}^i(t) = 0$. In this manner, the fidelity in the generation of the state can be estimated as follows: $\mathcal{F}(t) = |\langle W_N|\psi(t)\rangle|^2 \approx \left(N\,P_{\mathrm{e}}^i(t)\right)^{-1}|\sum_{n=1}^{N} c_n(t)|^2$.

Fig. 6(b) depicts a comparison between the fidelity predicted for the ideal case and in the sensitivity analysis. In the ideal case, the fidelity starts at $t = 0$ at the projection of the

initial state on the desired state, $\mathcal{F}(0) \approx \left|\langle W_N|\sigma_1^\dagger|0\rangle\right|^2 = N^{-1}$, and it monotonically increases until it approaches 1 after a transient time. By contrast, when nonidealities are taken into account, the average fidelity peaks at $\Gamma_{\mathrm{wg}} t_m = 1.9$ with a value of $\mathcal{F}(t) = 0.733$. Fig. 6(c) depicts the histograms of the evaluated fidelities at $\Gamma_{\mathrm{wg}} t_m = 1.9$ and $\Gamma_{\mathrm{wg}} t_o = 3$, the later being a time point where the transient decay has already finished. The figures reveal that predicted fidelities exhibit a quasi-normal distribution, centered around its average values 0.733 and 0.672, respectively, highlighted with a vertical red line, excluding the existence of pathological configurations that might dramatically degrade the performance of the system.

Therefore, we conclude for the sensitivity analysis that the procedure is progressively degraded, but not conceptually forbidden, by the existence of different nonidealities in the system. Our results suggest that the generation of multi-qubit subradiant (maximally entangled) states could be experimentally validated, even though it is clear that a very high-quality setup would be required to obtain a relatively high fidelity. We remark that this is only one example of the many potential applications of the scheme based on *N*-port devices. Moreover, assessing the performance and potential application of the system for a quantum information or metrology systems would require a much-in-depth and specific analysis, including additional factors such as the efficiency of the detectors, excitation scheme, bandwidth and similarity of the emitters, which is left for future efforts.

VI. Conclusions - In conclusion, we proposed the use of multiport devices to complement waveguide QED setups, and thus exploit some of the methodologies of the communication network systems in the field of reservoir and quantum state engineering. As a particular example of the potential of this approach, we have demonstrated theoretically the possibility of exciting multi-qubit subradiant, maximally entangled states, with potential applications in quantum information processing, lasing and sensing. Further, we showed theoretically that this concept can be implemented, for instance, by using EMNZ waveguide hubs and conventional circulators. Both devices could be implemented in a variety of platforms and/or physical systems. In addition, different multi-port devices could be utilized for the same task. In a general sense, our theoretical results serve to indicate that part of the complexity of quantum state engineering tasks can be transferred to the design of multiport devices. We emphasize that more sophisticated protocols could be developed with multi-level emitters and/or addressing each of the QEs with a dedicated laser.

Acknowledgments - The authors would like to acknowledge partial support from the Vannevar Bush Faculty Fellowship program sponsored by the Basic Research Office of the Assistant Secretary of Defense for Research and Engineering and funded by the Office of Naval Research through grant N00014-16-1-2029, and the partial support from the US Air Force Office of Scientific Research (AFOSR) Multidisciplinary University Research

Initiative (MURI) Award No. FA9550-12-1-0488. I.L. acknowledges support from Juan de la Cierva – Incorporación Fellowship.

Appendix A: Derivation of the quantum master equation - The basis of our following derivations is the macroscopic QED formalism introduced in previous works [36–38]. Specifically, we consider a system composed of *N* identical quantum emitters (QEs), modeled as two-level $\{|e_n\rangle, |g_n\rangle\}$ systems with transition frequency ω_0 (including the medium-assisted Lamb-shift) and transition dipole moment $\mathbf{p}_\mathrm{n} = \langle \mathrm{e_n}|\hat{\mathbf{p}}_\mathrm{n}|\mathrm{g_n}\rangle$. We assume that the QEs interact via a common inhomogenous, lossy and dispersive photonic environment, characterized by relative permittivity $\varepsilon(\mathbf{r},\omega) = \varepsilon_\mathrm{R}(\mathbf{r},\omega) + \mathrm{i}\varepsilon_\mathrm{I}(\mathbf{r},\omega)$ and relative permeability $\mu(\mathbf{r},\omega) = \mu_\mathrm{R}(\mathbf{r},\omega) + \mathrm{i}\mu_\mathrm{I}(\mathbf{r},\omega)$. The associated Hamiltonian in the interaction picture, $\hat{\mathrm{H}} = \hat{\mathrm{H}}_0 + \hat{\mathrm{H}}_\mathrm{I}$, includes the ensemble of QEs, the EM fields - matter system, as well as their interaction by means of electric dipole transitions:

$$\hat{\mathrm{H}}_0 = \sum_{\mathrm{n}=1}^{\mathrm{N}} \hbar\omega_0 \sigma_\mathrm{n}^\dagger \sigma_\mathrm{n} + \sum_{q=e,m} \int \mathrm{d}^3\mathrm{r}' \int \mathrm{d}\omega \;\; \hbar\omega\, \hat{\mathbf{f}}_q^\dagger(\mathbf{r}',\omega)\cdot\hat{\mathbf{f}}_q(\mathbf{r}',\omega) \tag{A.1}$$

$$\hat{\mathrm{H}}_\mathrm{I}(\mathrm{t}) = -\sum_{\mathrm{n}=1}^{\mathrm{N}} \left[\mathbf{p}_\mathrm{n}\cdot\mathbf{E}(\mathbf{r}_\mathrm{n},\mathrm{t})\sigma_\mathrm{n}^\dagger e^{i\omega_0 t} + \mathrm{h.c.}\right] \tag{A.2}$$

Here, $\sigma_\mathrm{n} = |\mathrm{g_n}\rangle\langle\mathrm{e_n}|$ is the lowering operator of the *n-th* QE, and $\hat{\mathbf{f}}_q(\mathbf{r}',\omega)$, $q = e,m$ are polaritonic operators representing excitations of the EM fields – matter system. The latter satisfy the commutation relations: $\left[\hat{\mathbf{f}}_\mathrm{p}(\mathbf{r},\omega), \hat{\mathbf{f}}_q^\dagger(\mathbf{r}',\omega')\right] = \mathbf{1}\,\delta_{pq}\delta(\mathbf{r}-\mathbf{r}')\delta(\omega-\omega')$ and $\left[\hat{\mathbf{f}}_\mathrm{p}(\mathbf{r},\omega), \hat{\mathbf{f}}_\mathrm{q}(\mathbf{r}',\omega')\right] = \mathbf{0}$. The electric field operator is $\hat{\mathbf{E}}(\mathbf{r},\mathrm{t}) = \int d\omega\, e^{-i\omega t}\,\hat{\mathbf{E}}(\mathbf{r},\omega) + \mathrm{h.c.}$, where $\hat{\mathbf{E}}(\mathbf{r},\omega) = \sum_{\mathrm{q=e,m}} \int d^3 r\, \mathbf{G}_\mathrm{q}(\mathbf{r},\mathbf{r}',\omega)\cdot\hat{\mathbf{f}}_\mathrm{q}(\mathbf{r}',\omega)$. We define the dyadic functions $\mathbf{G}_\mathrm{e}(\mathbf{r},\mathbf{r}',\omega) = \mathrm{i}\frac{\omega^2}{c^2}\sqrt{\frac{\hbar}{\pi\varepsilon_0}\varepsilon_I(\mathbf{r}',\omega)}\,\mathbf{G}(\mathbf{r},\mathbf{r}',\omega)$ and $\mathbf{G}_\mathrm{m}(\mathbf{r},\mathbf{r}',\omega) = -\mathrm{i}\frac{\omega}{c}\sqrt{\frac{\hbar}{\pi\varepsilon_0}\frac{\mu_I(\mathbf{r}',\omega)}{|\mu(\mathbf{r}',\omega)|^2}}\,\mathbf{G}(\mathbf{r},\mathbf{r}',\omega)\times\overleftarrow{\nabla}$, where $\mathbf{G}(\mathbf{r},\mathbf{r}',\omega)$ is the classical Green dyadic function of the background medium.

We follow an analysis similar to [14,72] in order to derive the quantum master equation describing the dynamics of the reduced density matrix for the QE system, $\rho_S = \mathrm{Tr}_B\{\rho\}$, and the coupling parameters J_{nm}. Note that in the main text we drop the *S* sub-index for the sake of brevity. The dynamics of the system are given by the interaction picture Von Neumann equation: [14] $i\hbar\partial_t\rho = \left[\hat{\mathrm{H}}_\mathrm{I}(\mathrm{t}), \rho(t)\right]$. Assuming that the relaxation of the background is much faster than that of the QE system, and that the influence of the quantum emitter on the system is small (Born-Markov approximation), we can derive the following integro-differential equation for the dynamics of the reduced density matrix ρ_S [14]

$$\partial_t \rho_S(t) = -\int_0^\infty ds\ \mathrm{Tr_B}\left\{\left[\widehat{\mathrm{H}}_\mathrm{I}(\mathrm{t}), \left[\widehat{\mathrm{H}}_\mathrm{I}(\mathrm{t}-\mathrm{s}), \rho_\mathrm{S}(\mathrm{t}) \otimes \rho_\mathrm{B}\right]\right]\right\} \tag{A.1}$$

By introducing (A.2) and evaluating Tr_B, we obtain a master equation in Linblad form [14]

$$\partial_t \rho_S = \mathcal{L}\{\rho_S\} = \sum_{n,m} J_{nm}\left(\sigma_n \rho_S \sigma_m^\dagger - \rho_S \sigma_m^\dagger \sigma_n\right) + h.c. \tag{A.2}$$

Here, the J_{nm} factors are derived as coupling parameters, given by

$$J_{nm} = \int_0^\infty ds\ \left(e^{-i\omega_0 s} + e^{i\omega_0 s}\right)\langle \mathbf{p}_\mathrm{n} \cdot \mathbf{E}(\mathbf{r}_\mathrm{n}, \mathrm{t}) \mathbf{p}_\mathrm{m} \cdot \mathbf{E}(\mathbf{r}_\mathrm{m}, \mathrm{t}-\mathrm{s})\rangle \tag{A.3}$$

Note that, following [72], we keep the counter rotating terms. Next, we assume that the background field + matter systems is on its vacuum state (i.e., the QE system have a negligible impact on the background). Consequently, and applying the completeness relationship of the Green's function we obtain

$$\langle \mathbf{p}_\mathrm{n} \cdot \mathbf{E}(\mathbf{r}_\mathrm{n}, \mathrm{t})\ \mathbf{p}_\mathrm{m} \cdot \mathbf{E}(\mathbf{r}_\mathrm{m}, \mathrm{t}-\mathrm{s})\rangle = \frac{\hbar}{\pi\varepsilon_0} \int_0^\infty \mathrm{d}\omega\ \frac{\omega^2}{\mathrm{c}^2}\ \mathrm{e}^{-\mathrm{i}\omega\mathrm{s}}\ \mathbf{p}_\mathrm{n} \cdot \mathrm{Im}\mathbf{G}(\mathbf{r}_\mathrm{n}, \mathbf{r}_\mathrm{m}, \omega) \cdot \mathbf{p}_\mathrm{m} \tag{A.5}$$

In this manner, the coupling parameters can be written as

$$J_{nm} = \frac{\hbar}{\pi\varepsilon_0}\int_0^\infty \mathrm{d}\omega\ \frac{\omega^2}{\mathrm{c}^2}\ \ \mathbf{p}_\mathrm{n} \cdot \mathrm{Im}\mathbf{G}(\mathbf{r}_\mathrm{n}, \mathbf{r}_\mathrm{m}, \omega) \cdot \mathbf{p}_\mathrm{m} \int_0^\infty ds\ \left(e^{-i(\omega_0+\omega)s} + e^{i(\omega_0-\omega)s}\right) \tag{A.6}$$

Next, recalling the identity $\int_0^\infty ds\ e^{ias} = \pi\delta(a) + iP\frac{1}{a}$, we obtain

$$\begin{aligned} J_{nm} &= \frac{\hbar}{\varepsilon_0}\frac{\omega_0^2}{\mathrm{c}^2}\ \mathbf{p}_\mathrm{n} \cdot \mathrm{Im}\mathbf{G}(\mathbf{r}_\mathrm{n}, \mathbf{r}_\mathrm{m}, \omega_0) \cdot \mathbf{p}_\mathrm{m} \\ &+ \frac{\mathrm{i}\hbar}{\pi\varepsilon_0}\mathrm{P}\int_0^\infty \mathrm{d}\omega\ \frac{\omega^2}{\mathrm{c}^2}\ \left\{\frac{\mathbf{p}_\mathrm{n} \cdot \mathrm{Im}\mathbf{G}(\mathbf{r}_\mathrm{n}, \mathbf{r}_\mathrm{m}, \omega) \cdot \mathbf{p}_\mathrm{m}}{\omega_0 - \omega} - \frac{\mathbf{p}_\mathrm{n} \cdot \mathrm{Im}\mathbf{G}(\mathbf{r}_\mathrm{n}, \mathbf{r}_\mathrm{m}, \omega) \cdot \mathbf{p}_\mathrm{m}}{\omega_0 + \omega}\right\} \end{aligned} \tag{A.7}$$

In addition, since $G_{ij}^*(\boldsymbol{r}_n, \boldsymbol{r}_m, \omega) = G_{ij}(\boldsymbol{r}_n, \boldsymbol{r}_m, -\omega^*)$ [36], we can simply write

$$J_{nm} = \frac{\hbar}{\varepsilon_0}\frac{\omega_0^2}{\mathrm{c}^2}\ \mathbf{p}_\mathrm{n} \cdot \mathrm{Im}\mathbf{G}(\mathbf{r}_\mathrm{n}, \mathbf{r}_\mathrm{m}, \omega_0) \cdot \mathbf{p}_\mathrm{m} + \frac{\mathrm{i}\hbar}{\pi\varepsilon_0}\mathrm{P}\int_{-\infty}^\infty \mathrm{d}\omega\ \frac{\omega^2}{\mathrm{c}^2}\ \frac{\mathbf{p}_\mathrm{n} \cdot \mathrm{Im}\mathbf{G}(\mathbf{r}_\mathrm{n}, \mathbf{r}_\mathrm{m}, \omega) \cdot \mathbf{p}_\mathrm{m}}{\omega_0 - \omega} \tag{A.8}$$

To finalize, applying Kramers-Kronig relations for any causal function $f(\omega)$, $\mathrm{Re}\{f(\omega_0)\} = \frac{1}{\pi}\,\mathrm{P}\int_{-\infty}^{\infty} \mathrm{d}\omega\, \frac{\mathrm{Im}\{f(\omega)\}}{\omega-\omega_0}$ we obtain the simple form

$$J_{nm} = -i\frac{\hbar}{\varepsilon_0}\frac{\omega_0^2}{\mathrm{c}^2}\mathbf{p}_\mathrm{n}\cdot\mathbf{G}(\mathbf{r}_\mathrm{n},\mathbf{r}_\mathrm{m},\omega_0)\cdot\mathbf{p}_\mathrm{m} \tag{A.9}$$

Appendix B: Quantum master equation for the single excitation case - In the single excitation case, the state of the QE system reduces to $|\psi_S(t)\rangle = \sum_{p=1}^{N} c_p(t)\ \left|e_p\right\rangle + c_g(t)|0\rangle$. The associated QE-system density matrix is thus given by

$$\begin{aligned}\rho_S(t) = |\psi_S(t)\rangle\langle\psi_S(t)| = \sum_{p=1}^{N}\sum_{q=1}^{N} c_p(t)\,c_q^*(t)\,\left|e_p\right\rangle\left\langle e_q\right| + \left|c_g(t)\right|^2|0\rangle\langle 0| \\ + \sum_{p=1}^{N} c_p(t)c_g^*\ \left|e_p\right\rangle\langle 0| + \sum_{q=1}^{N} c_g(t)c_q^*\ |0\rangle\left\langle e_q\right|\end{aligned} \tag{B.1}$$

Combining this density matrix with the QME we obtain the following generalized optical Bloch equations describing the decay of the QE system:

$$\partial_t\left\{\left|c_g(t)\right|^2\right\} = \sum_{n=1}^{N}\sum_{m=1}^{N}[J_{nm}c_nc_m^* + J_{nm}^*c_mc_n^*] \tag{B.2}$$

$$\partial_t\{c_g(t)c_m^*(t)\} = -\sum_{m=1}^{N} J_{nm}c_gc_m^* \tag{B.3}$$

$$\partial_t\{c_a(t)c_b^*(t)\} = -\sum_{m=1}^{N}[J_{bm}c_ac_m^* + J_{am}^*c_mc_b^*] \tag{B.4}$$

To finalize, since these generalized optical Bloch equation must be satisfied for all a, b coefficients, each $c_n(t)$ coefficient is given by the solution to $\partial_t\{c_n(t)\} = \sum_{m=1}^{N} K_{nm}c_m$, with $K_{nm} = -J_{nm}^*$. Equivalently, we can write this equation in matrix form

$$\partial_t\boldsymbol{c}(t) = \boldsymbol{K}\cdot\boldsymbol{c}(t) \tag{B.5}$$

where $\boldsymbol{c} = [c_1(t),\dots,c_N(t)]^{\boldsymbol{T}}$ is a vector gathering all probability amplitudes, and $\boldsymbol{K}$ is a square $N\times N$ composed by the K_{nm} elements.

Appendix C: Solution for epsilon-and-mu-near-zero (EMNZ) hubs

Here we derive explicit expressions for the time-evolution of the probability amplitudes of the excited states $c_n(t)$ for $n = 1, \dots, N$, for an EMNZ hub. As derived in the main text, if we set $k_{\mathrm{wg}}d = \pi$, the elements of the $\boldsymbol{K}$ reduce to $K_{nn} = -\Gamma_{\mathrm{wg}}(N-1)/N \ \ \forall n$ and $K_{nm} = \Gamma_{\mathrm{wg}}/N$ for $n \neq m$. Subsequently, equation (B.5) can be explicitly written as follows

$$\partial_t c_n(t) = -\frac{\Gamma_{\mathrm{wg}}}{N}\left[(N-1)c_n(t) - \sum_{m\neq n} c_m(t)\right] \ \ \forall n \tag{C.1}$$

Next, we observe that due to the symmetry of the coupling parameters (the coupling is independent of the position of the ports), the probability amplitudes (and their time evolution) of those two-level systems sharing the same initial condition is identical. Therefore, assuming the initial state $|\psi(0)\rangle = \sigma_1^{\dagger}|0\rangle$, then we have $c_2(t) = c_3(t) = \cdots = c_N(t)$, and $c_1(t) \neq c_2(t)$. Thus, the above system of *N* differential equations reduces to two coupled differential equations

$$\partial_t c_1(t) = -\frac{N-1}{N}\,\Gamma_{\mathrm{wg}}\,[c_1(t) - c_2(t)] \tag{C.2}$$

$$\partial_t c_2(t) = -\frac{\Gamma_{\mathrm{wg}}}{N}\,[c_2(t) - c_1(t)] \tag{C.3}$$

Here it is already clear that $c_1(t) = c_2(t)$ is a stationary state of the system for which $\partial_t c_1(t) = 0$ and $\partial_t c_2(t) = 0$. In any event, the general solution to the coupled equations is $c_1(t) = A + Be^{-\Gamma_{\mathrm{wg}}t}$ and $c_2(t) = A - B(N-1)^{-1}e^{-\Gamma_{wg}t}$. The value of the constants A and B, and thus the particular solution, is found by imposing the initial conditions $c_1(0) = 1$ and $\partial_t c_1(0) = -N^{-1}(N-1)\,\Gamma_{\mathrm{wg}}$, leading to $A = N^{-1}$ and $B = N^{-1}(N-1)$.

Appendix D: Solution for nonreciprocal circulators **-** An ideal nonreciprocal circulator is defined as a *N*-port device allowing for nonreciprocal one-to-one interactions between the two-level systems. In this manner, the diagonal (self)coupling parameters are given by $K_{nn} = -\frac{\Gamma_{\mathrm{wg}}}{2} \ \forall n$, while the only nonzero nondiagonal coupling parameters are $K_{1N} = \frac{\Gamma_{\mathrm{wg}}}{2}$ and $K_{n(n-1)} = \frac{\Gamma_{\mathrm{wg}}}{2}$ for $n > 1$. Therefore, equation (B.5) an be written in a recursive manner as follows

$$\partial_t c_n(t) = -\frac{\Gamma_{\mathrm{wg}}}{2}\,[c_n(t) - c_{n-1}(t)] \quad \text{for} \quad n \geq 2 \tag{D.1}$$

and

$$\partial_t c_1(t) = -\frac{\Gamma_{\mathrm{wg}}}{2}\,[c_1(t) - c_N(t)] \tag{D.2}$$

These equations can be rearranged to compactly write

$$c_n(t) = \left(1 + 2\frac{\partial_t}{\Gamma_{\mathrm{wg}}}\right)^{N+1-n} c_1(t) \quad \forall n \tag{D.3}$$

Including, for example $c_1(t) = \left(1 + 2\frac{\partial_t}{\Gamma_{\mathrm{wg}}}\right)^{N} c_1(t)$. Next, we try solutions of the form $c_1(t) = e^{-\gamma t}$, with $\gamma \in \mathbb{R}$, leading to the characteristic equation $\left(1 - 2\frac{\gamma}{\Gamma_{\mathrm{wg}}}\right)^{N} = 1$, with solutions $\gamma = \frac{\Gamma_{\mathrm{wg}}}{2}\left(1 - e^{im2\pi/N}\right)$ for $m = 0,1,\ldots,N-1$. Then, by imposing the initial conditions for a single excitation, i.e., $c_1(0) = 1$ and $c_n(0) = 0$ for $n \geq 2$, onto the general solution constructed with all aforementioned eigenvalues, the time evolution of the probability amplitudes can be written as

$$c_n(t) = \frac{1}{\mathrm{N}}\sum_{\mathrm{m}=0}^{\mathrm{N}-1} \exp\left[-\frac{\Gamma_{\mathrm{wg}}}{2}\left(1 - e^{im2\pi/N}\right)\mathrm{t} + \mathrm{i}m2\pi\frac{N-n+1}{N}\right] \quad \forall n \tag{D.4}$$

References

[1] R. Horodecki, P. Horodecki, M. Horodecki, and K. Horodecki, Rev. Mod. Phys. **81**, 865 (2009).

[2] M. A. Nielsen and I. L. Chuang, *Quantum Computation and Quantum Information* (Cambridge University Press, 2010).

[3] J. I. Cirac, P. Zoller, H. J. Kimble, and H. Mabuchi, Phys. Rev. Lett. **78**, 3221 (1997).

[4] L. M. Duan, M. D. Lukin, J. I. Cirac, and P. Zoller, Nature **414**, 413 (2001).

[5] A. Reiserer and G. Rempe, Rev. Mod. Phys. **87**, 1379 (2015).

[6] V. Giovannetti, S. Lloyd, and L. Maccone, Science **306**, 1330 (2004).

[7] A. V. Akimov, A. Mukherjee, C. L. Yu, D. E. Chang, A. S. Zibrov, P. R. Hemmer, H. Park, and M. D. Lukin, Nature **450**, 402 (2007).

[8] C. W. Wong, J. Gao, J. F. McMillan, F. W. Sun, and R. Bose, Photonics Nanostructures - Fundam. Appl. **7**, 47 (2009).

[9] Q. Quan, I. Bulu, and M. Lončar, Phys. Rev. A **80**, 011810(R) (2009).

[10] A. F. van Loo, A. Fedorov, K. Lalumiere, B. C. Sanders, A. Blais, and A. Wallraff, Science **342**, 1494 (2013).

[11] M. Arcari, I. Söllner, A. Javadi, S. L. Hansen, S. Mahmoodian, J. Liu, H. Thyrrestrup, E. H. Lee, J. D. Song, S. Stobbe, and P. Lodahl, Phys. Rev. Lett. **113**,

93603 (2014).

[12] A. Goban, C.-L. Hung, J. D. Hood, S.-P. Yu, J. A. Muniz, O. Painter, and H. J. Kimble, Phys. Rev. Lett. **115**, 63601 (2015).

[13] A. Goban, C.-L. Hung, S.-P. Yu, J. D. Hood, J. . A. Muniz, J. H. Lee, M. J. Martin, A. C. McClung, K. S. Choi, D. E. Chang, O. Painter, and H. J. Kimble, Nat. Commun. **5**, 3808 (2014).

[14] H. P. Breuer and F. Petruccione, *The Theory of Open Quantum Systems* (Oxford University Press, 2002).

[15] B. Kraus, H. P. Büchler, S. Diehl, A. Kantian, A. Micheli, and P. Zoller, Phys. Rev. A **78**, 42307 (2008).

[16] S. Diehl, A. Micheli, A. Kantian, B. Kraus, H. P. Büchler, and P. Zoller, Nat. Phys. **4**, 878 (2008).

[17] F. Verstraete, M. M. Wolf, and J. Ignacio Cirac, Nat. Phys. **5**, 633 (2009).

[18] A. González-Tudela, D. Martin-Cano, E. Moreno, L. Martin-Moreno, C. Tejedor, and F. J. Garcia-Vidal, Phys. Rev. Lett. **106**, 20501 (2011).

[19] M. J. Kastoryano, F. Reiter, and A. S. Sørensen, Phys. Rev. Lett. **106**, 90502 (2011).

[20] D. Dzsotjan, A. S. Sørensen, and M. Fleischhauer, Phys. Rev. B **82**, 75427 (2010).

[21] R. Sokhoyan and H. A. Atwater, Prepr. Available http//arxiv.org/abs/1510.07071 1 (2015).

[22] C. Gonzalez-Ballestero, A. González-Tudela, F. J. Garcia-Vidal, and E. Moreno, Phys. Rev. B **92**, 155304 (2015).

[23] A. González-Tudela and D. Porras, Phys. Rev. Lett. **110**, 80502 (2013).

[24] K. Stannigel, P. Rabl, and P. Zoller, New J. Phys. **14**, 63014 (2012).

[25] H. Krauter, C. A. Muschik, K. Jensen, W. Wasilewski, J. M. Petersen, J. I. Cirac, and E. S. Polzik, Phys. Rev. Lett. **107**, 80503 (2011).

[26] F. Pastawski, L. Clemente, and J. I. Cirac, Phys. Rev. A **83**, 12304 (2011).

[27] K. G. H. Vollbrecht, C. A. Muschik, and J. I. Cirac, Phys. Rev. Lett. **107**, 120502 (2011).

[28] J. T. Barreiro, M. Müller, P. Schindler, D. Nigg, T. Monz, M. Chwalla, M. Hennrich, C. F. Roos, P. Zoller, and R. Blatt, Nature **470**, 486 (2011).

[29] V. Paulisch, H. J. Kimble, and A. González-Tudela, New J. Phys. **18**, 43041 (2016).

[30] A. González-Tudela, V. Paulisch, D. E. Chang, H. J. Kimble, and J. I. Cirac, Phys. Rev. Lett. **115**, 163603 (2015).

[31] David M. Pozar, *Microwave Engineering,4th Ed.* (JohnWiley & Sons, Inc., 2012).

[32] W. Dur, G. Vidal, and J. I. Cirac, Phys. Rev. A **62**, 62314 (2000).

[33] C. W. Hsu, B. Zhen, A. D. Stone, J. D. Joannopoulos, and M. Soljačić, Nat. Rev. Mater. **1**, 16048 (2016).

[34] Y. L. Lim and A. Beige, Phys. Rev. A **71**, 62311 (2005).

[35] G. N. M. Tabia, Phys. Rev. A **86**, 62107 (2012).

[36] W. Vogel and D.-G. Welsch, *Quantum Optics* (John Wiley & Sons, Berlin, 2006).

[37] B. Huttner and S. M. Barnett, Phys. Rev. A **46**, 4306 (1992).

[38] T. G. Philbin, New J. Phys. **12**, 123008 (2010).

[39] C. Aron, M. Kulkarni, and H. E. Türeci, Phys. Rev. X **6**, 11032 (2016).

[40] I. Liberal and N. Engheta, Nat. Photonics **11**, 149 (2017).

[41] N. Engheta and R. W. Ziolkowski, *Metamaterials: Physics and Engineering Explorations* (John Wiley & Sons, 2006).

[42] R. W. Ziolkowski, Phys. Rev. E **70**, 46608 (2004).

[43] N. Engheta, Science **340**, 286 (2013).

[44] I. Liberal and N. Engheta, Opt. Photonics News **27**, 26 (2016).

[45] A. M. Mahmoud and N. Engheta, Nat. Commun. **5**, 5638 (2014).

[46] I. Liberal, A. M. Mahmoud, Y. Li, B. Edwards, and N. Engheta, Science **355**, 1058 (2017).

[47] M. G. Silveirinha and N. Engheta, Phys. Rev. Lett. **97**, 157403 (2006).

[48] B. Edwards, A. Alù, M. E. Young, M. G. Silveirinha, and N. Engheta, Phys. Rev. Lett. **100**, 33903 (2008).

[49] I. Liberal and N. Engheta, Proc. Natl. Acad. Sci. USA **114**, 822 (2017).

[50] R. Fleury and A. Alù, Phys. Rev. B **87**, 201101 (2013).

[51] E. Shahmoon and G. Kurizki, Phys. Rev. A **87**, 33831 (2013).

[52] R. Sokhoyan and H. A. Atwater, Opt. Express **21**, 32279 (2013).

[53] I. Liberal and N. Engheta, Sci. Adv. **2**, e1600987 (2016).

[54] Y. Li and C. Argyropoulos, Opt. Express **24**, 26696 (2016).

[55] A. M. Mahmoud, I. Liberal, and N. Engheta, Opt. Mater. Express **7**, 415 (2017).

[56] (2016).

[57] X. Huang, Y. Lai, Z. H. Hang, H. Zheng, and C. T. Chan, Nat. Mater. **10**, 582 (2011).

[58] Y. Li, S. Kita, P. Muñoz, O. Reshef, D. I. Vulis, and M. Yin, Nat. Photonics **9**, 738 (2015).

[59] Y. Wu, J. Li, Z. Q. Zhang, and C. T. Chan, Phys. Rev. B **74**, 85111 (2006).

[60] D. Pozar, *Microwave Engineering*, 4th ed. (2009).

[61] E. F. Schloemann, Proc. IEEE **76**, 188 (1988).

[62] J. C. Palais, *Fiber Optic Communication 5th Ed* (Englewood Cliffs: Prentice Hall, 1988).

[63] *THORLABS, Www.thorlabs.com* (n.d.).

[64] Z. Wang and S. Fan, Opt. Lett. **30**, 1989 (2005).

[65] A. R. Davoyan and N. Engheta, New J. Phys. **15**, 83054 (2013).

[66] J. Petersen, J. Volz, and A. Rauschenbeutel, Science **346**, 67 (2014).

[67] I. Söllner, S. Mahmoodian, S. L. Hansen, L. Midolo, A. Javadi, G. Kiršanskė, T. Pregnolato, H. El-Ella, E. H. Lee, J. D. Song, S. Stobbe, and P. Lodahl, Nat. Nanotechnol. **10**, 775 (2015).

[68] C. Sayrin, C. Junge, R. Mitsch, B. Albrecht, D. O'Shea, P. Schneeweiss, J. Volz, and A. Rauschenbeutel, Phys. Rev. X **5**, 41036 (2015).

[69] M. Scheucher, A. Hilico, E. Will, J. Volz, and A. Rauschenbeutel, Science In Press (2016).

[70] R. Fleury, D. L. Sounas, C. F. Sieck, M. R. Haberman, and A. Alù, Science **343**, 516 (2014).

[71] M. Arcari, I. Söllner, A. Javadi, S. L. Hansen, S. Mahmoodian, J. Liu, H. Thyrrestrup, E. H. Lee, J. D. Song, S. Stobbe, and P. Lodahl, Phys. Rev. Lett. **93603**, 1 (2014).

[72] A. González-Tudela and D. Porras, Phys. Rev. Lett. **110**, 80502 (2013).

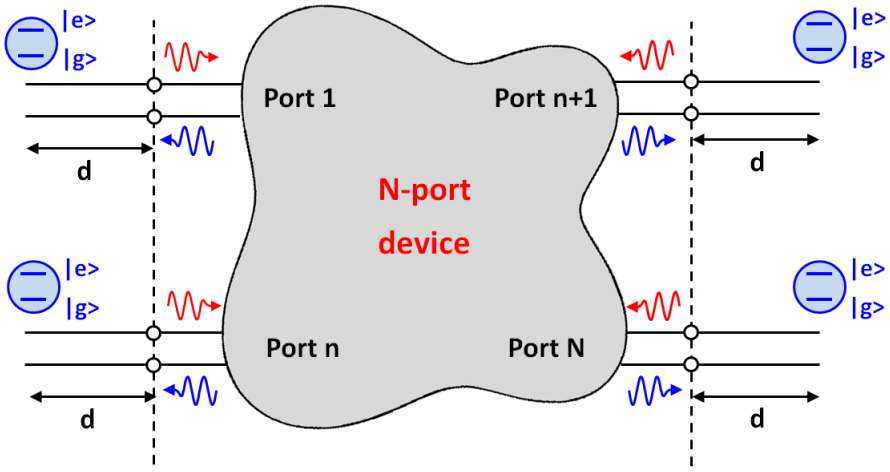

$$\mathbf{S} = \begin{bmatrix} S_{11} & S_{12} & \cdots & S_{1N} \\ S_{21} & S_{22} & \cdots & \cdots \\ \cdots & \cdots & \cdots & \cdots \\ S_{N1} & S_{N2} & \cdots & S_{NN} \end{bmatrix}$$

Fig. 1. Conceptual sketch of an N-port waveguide device. *Sketch of a device: two-level systems are coupled to N single-mode waveguides connected via an N-port hub. The response of the device is characterized by its scattering (S-parameter) matrix, whose elements represent the reflection and transmission coefficients between the different ports.*

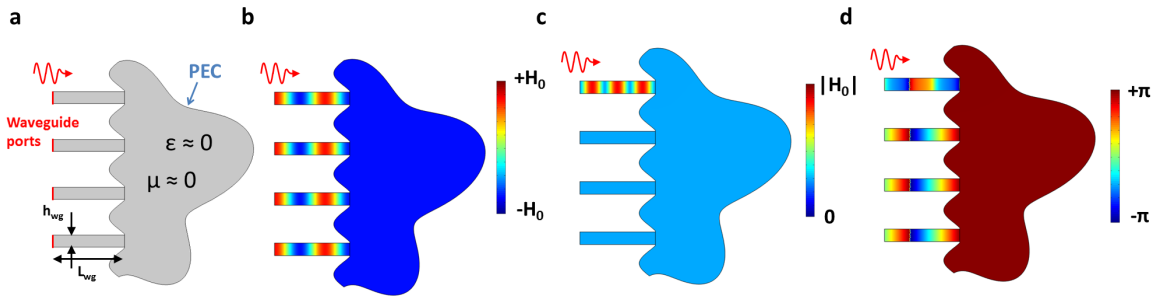

Fig. 2: Wave propagation through an N-port EMNZ hub. a, *Sketch of the simulation setup: a two-dimensional (2D) EMNZ body ($\mu = \varepsilon = 0.001$) of arbitrary shape is closed by a perfect electric conductor (PEC) wall and connected to the outside via four identical 2D waveguides (filled with air) of height $h_{wg} = 0.25\lambda_0$ and length $L_{wg} = 1.5\lambda_0$, terminated into waveguide ports supporting a TEM mode.* ***b,*** *Snapshot,* ***c****, magnitude and* ***d****, phase of the magnetic field excited when a wave is introduced into the system via the top port. The field distributions demonstrate that the waves outgoing the three remaining ports are identical in magnitude and phase.*

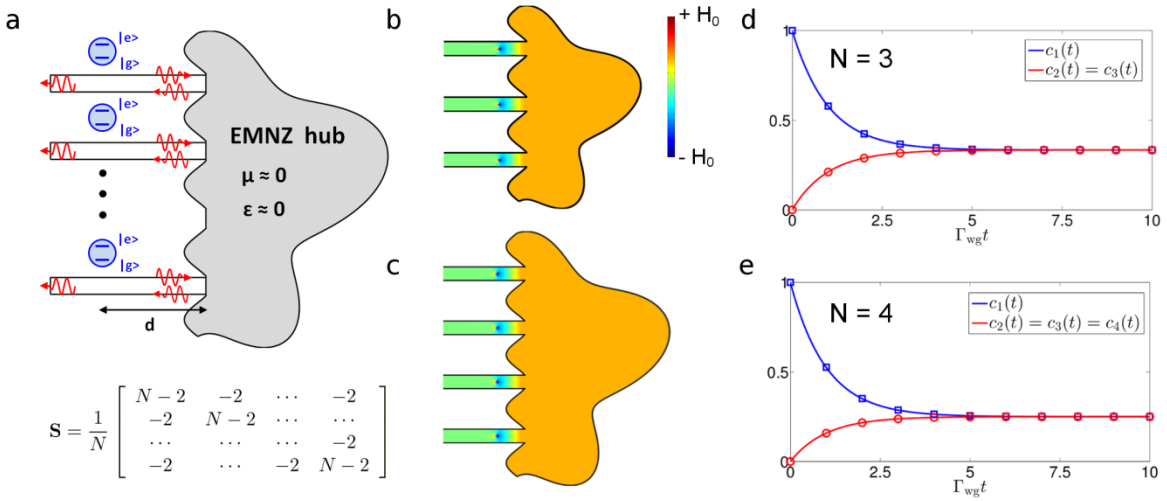

Fig. 3. N-port epsilon-and-mu-near-zero (EMNZ) two-dimensional (2D) waveguide hubs. ***(a)*** *Sketch and scattering matrix of a generic EMNZ waveguide hub.* ***(b)-(c)*** *Snapshot of the magnetic field (H_z component), showing no emitted power exiting the system and thus evidencing the excitation of a dark state, when the QEs are replaced by a classical 2D point electric dipoles emitting in phase, for* ***(b)*** *$N = 3$ and* ***(c)*** *$N = 4$ port devices.* ***(d)-(e)*** *Numerical (solid line) and analytical (markers) solutions to the time-evolution of the probability amplitude of the individual QEs excited states, $c_n(t)$, located at a distance $k_{wg}d = \pi$ of the ports of a EMNZ waveguide hub with* ***(d)*** *N=3 and* ***(e)*** *N=4 ports.*

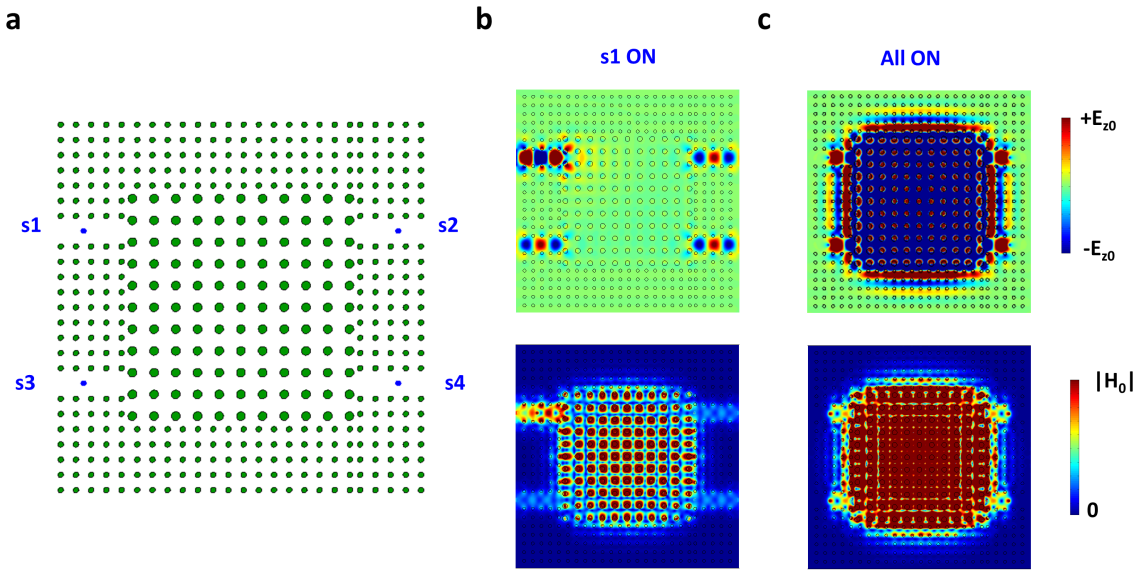

Fig. 4. Idea for a possible all-dielectric implementation of a four-port EMNZ hub. (a)*, Sketch of the geometry: an EMNZ region may be considered with a photonic crystal (PC) exhibiting a Dirac cone at k = 0 following* [57] and [55] *(rectangular lattice with period* $a_1 = 0.56\lambda_0$*, of dielectric rods of radius* $r_1 = 0.2a_1$ *and relative permittivity* $\varepsilon_r = 12.5$*). This region is closed by another PC (*$a_2 = 0.392\lambda_0$*,* $r_2 = 0.18a_2$*) exhibiting a complete band-gap at the EMNZ frequency. The system is excited by four different sources (s1, s2, s3 and s4, shown as blue dots), modeled as out-of-plane current lines (* $\boldsymbol{J} = \hat{\mathbf{z}}I$*). **(b)**, Snapshot of the electric field* E_z *(top), and magnetic field magnitude* $|\boldsymbol{H}|$*, excited when only one source (s1, positioned in the top left waveguide) is activated. The field distributions confirm that the signals outgoing the other three ports are identical in magnitude and phase. **(c)**, Same as **b**, but when all sources are activated at the same time. In this case, the electric field distribution evidences the excitation of a 'dark state', with no outgoing waves (nor power) exiting the system.*

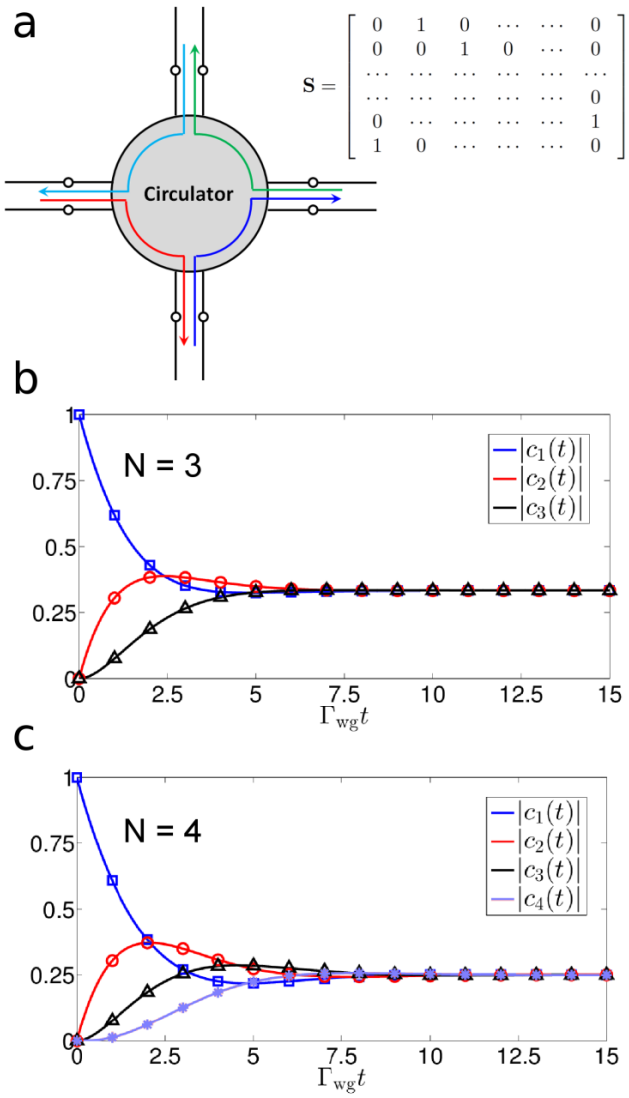

Fig. 5. Entanglement generation in N-port (nonreciprocal) circulators. ***(a)*** *Sketch and scattering matrix of the ideal device.* ***(b)-(c)*** *Numerical (solid line) and analytical (markers) solutions to the time-evolution of the probability amplitude of the individual QEs excited states located at distance* $k_{wg}d = \pi/2$ *of the ports of a circulator with* ***(b)*** *N=3 and* ***(c)*** *N=4 ports.*

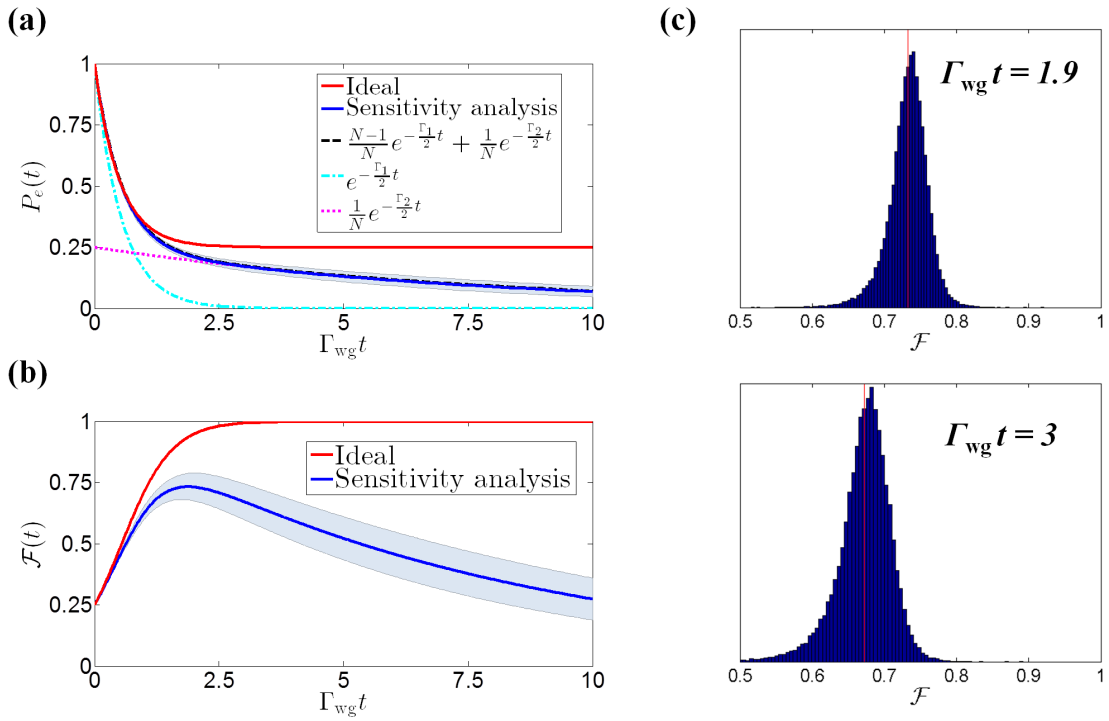

Fig. 6 Sensitivity analysis for a four-port EMNZ hub. ***(a)*** *Comparison between the time evolution of the probability of the excitation remaining in the QE system,* $P_e(t) = \sum_{n=1}^{N}|c_n(t)|^2$*, predicted in the ideal case and in the sensitivity analysis. Light blue background indicated the 95% confidence interval. For comparison we also include reference lines corresponding to the transient, subradiant and combined exponential decays,* $e^{-\Gamma_1 t}$*,* $\frac{1}{N}e^{-\Gamma_2 t}$ *and* $\frac{N-1}{N}e^{-\Gamma_1 t}+\frac{1}{N}e^{-\Gamma_2 t}$*, respectively, with* $\Gamma_1 = 1.85\,\Gamma_{wg}$ *and* $\Gamma_2 = 0.125\,\Gamma_{wg}$*.* ***(b)*** *Comparison between the time evolution of the fidelity,* $\mathcal{F} = |\langle W_N|\psi(t)\rangle|^2$*, predicted in the ideal case and average value in the sensitivity analysis.* ***(c)*** *Histograms of the fidelities predicted in the sensitivity analysis at the time points* $\Gamma_{wg}t = 1.9$*, corresponding to the peak of the average fidelity, and* $\Gamma_{wg}t = 3$*, corresponding to a point after the transient time. Average values are indicated with a vertical red line.*